

Accepted Manuscript

RuCo NPs supported on MIL-96(Al) as highly active catalysts for the hydrolysis of ammonia borane

Di Lu, Guofeng Yu, Yue Li, Menghuan Chen, Yaxi Pan, Liqun Zhou, Kunzhou Yang, Xing Xiong, Peng Wu, Qinghua Xia



PII: S0925-8388(16)33163-2

DOI: [10.1016/j.jallcom.2016.10.055](https://doi.org/10.1016/j.jallcom.2016.10.055)

Reference: JALCOM 39222

To appear in: *Journal of Alloys and Compounds*

Received Date: 25 June 2016

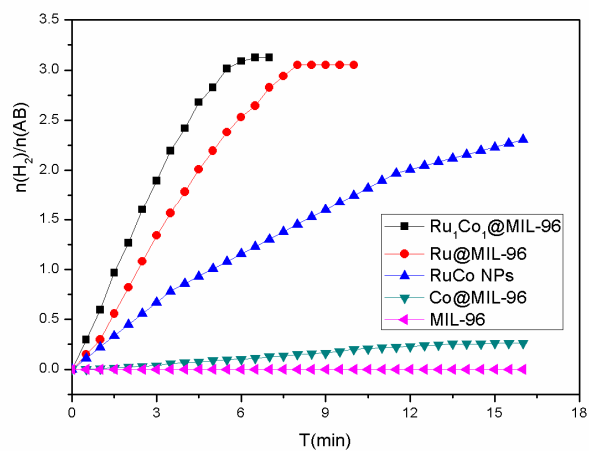
Revised Date: 29 September 2016

Accepted Date: 6 October 2016

Please cite this article as: D. Lu, G. Yu, Y. Li, M. Chen, Y. Pan, L. Zhou, K. Yang, X. Xiong, P. Wu, Q. Xia, RuCo NPs supported on MIL-96(Al) as highly active catalysts for the hydrolysis of ammonia borane, *Journal of Alloys and Compounds* (2016), doi: 10.1016/j.jallcom.2016.10.055.

This is a PDF file of an unedited manuscript that has been accepted for publication. As a service to our customers we are providing this early version of the manuscript. The manuscript will undergo copyediting, typesetting, and review of the resulting proof before it is published in its final form. Please note that during the production process errors may be discovered which could affect the content, and all legal disclaimers that apply to the journal pertain.

Graphical abstract:



Hydrogen generation rate from the hydrolysis of AB: different Ru, Co based catalysts.

RuCo NPs supported on MIL-96(Al) as highly active catalysts for the hydrolysis of ammonia borane

Di Lu^a, Guofeng Yu^b, Yue Li^a, Menghuan Chen^a, Yaxi Pan^a, Liquan Zhou^{a,*}, Kunzhou Yang^a, Xing Xiong^a, Peng Wu^a, Qinghua Xia^a

^aHubei Collaborative Innovation Center for Advanced Organic Chemical Materials, Ministry of Education Key Laboratory for the Synthesis and Application of Organic Functional Molecules, College of Chemistry and Chemical Engineering, Hubei University, Wuhan 430062, PR China

^bHubei Engineering University, Xiaogan 432000, PR China

Abstract: Bimetallic RuCo nanoparticles (NPs) were successfully deposited on the highly porous and hydrothermally stable nanofibrous metal-organic framework MIL-96(Al) by using a simple liquid impregnation strategy, and the powder XRD, FT-IR, BET, TEM, EDX, ICP-AES and XPS were employed to characterize the structure, size, composition and loading metal electronic states of the RuCo@MIL-96 catalysts. The catalytic property of RuCo@MIL-96 for hydrogen generation from the hydrolysis of ammonia borane (AB) at room temperature was investigated. The results show that Ru₁Co₁@MIL-96 exhibits much enhanced catalytic activity compared with monometallic Ru, Co counterparts loadings and RuCo NPs due to the uniform distribution of metal NPs and synergetic effect between Ru and Co particles as well as bi-functional effects between RuCo NPs and the host of MIL-96. The turn over frequency (TOF) value of the Ru₁Co₁@MIL-96 catalyst is determined to be 320.7 mol H₂ min⁻¹ (mol Ru)⁻¹, which is higher than most of the reported TOF values for the same reaction, and the activation energy (E_a) is 36.0 kJ mol⁻¹. Moreover, this catalyst exhibits satisfied durability after five cycles for the hydrolytic

* Corresponding authors.

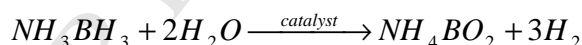
E-mail addresses:ldff2016@163.com (D. Lu), zhoulq2003@163.com (L. Zhou).

dehydrogenation of ammonia borane.

Keywords: MIL-96 RuCo loading catalysts Ammonia borane Hydrogen storage

1.Introduction

Hydrogen, producing only water as a byproduct, has been considered to be the most promising carrier for alternative energy applications [1]. But for the development of hydrogen energy economy, searching for safe and efficient hydrogen storage materials remains one of the most challenging barriers [2]. Various hydrogen storage approaches are currently being investigated, including metal hydrides [3], sorbent materials [4], and chemical hydride systems [5]. Among the chemical hydrides, ammonia borane (NH_3BH_3 , denoted as AB) appears to be an appropriate hydrogen storage material because of its high hydrogen content of 19.6wt%, excellent stability under ambient conditions, and environmental benign [6]. The release of hydrogen from AB can be obtained through thermal dehydrogenation in the solid state [7], hydrolysis [8] or methanolysis in solution [9]. With an appropriate catalyst, the hydrolysis of AB can release as much as 3 mol of hydrogen per mol of AB. The catalytic hydrolysis reaction can be briefly expressed as follows [10]:



Heterogeneous catalysts containing noble metal NPs exhibited good catalytic property toward AB hydrolysis, with ruthenium NPs considered as one of the most effective catalysts in the system [11]. However, the widespread utilization of noble metal-based catalysts was hindered by their high price and limited abundance. Bimetallic NPs consisting of noble metal and inexpensive first-row transition metal have exhibited good catalytic performance in many fields mainly due to the synergistic interactions between two or three different metals [12-14]. On the other hand, due to the high specific surface area and tunable pore size, metal-organic frameworks (MOFs) have attracted growing attention in the application of gas sorption and storage [15], drug delivery [16], and molecular separation [17]. The

metal NPs anchored by MOFs are expected to improve the catalytic activity and stability, since MOFs with confined pores and cavities could control the growth and dispersion of metal NPs and restrain the migration and aggregation of metal NPs. Up to now, a series of metal NPs@MOFs catalysts were tested for hydrolytic dehydrogenation of AB, such as Ru@MIL-101 [18], Pd@MIL-101 [19], Ru@MIL-96(Al) [20], RhNi@ ZIF-8 [21], RuCuCo@MIL-101 [14], CuCo@MIL-101 [22] and so on. Therefore, developing a facile one-step route to construct the bimetallic or trimetallic NPs in MIL-96 with high catalytic activities is highly desirable.

Herein, for the first time, the catalyst of bimetallic RuCo NPs immobilized in MIL-96(Al) has been successfully synthesized. For comparison with the RuCo@MIL-96 catalytic activities for hydrolysis of AB at room temperature, monometallic Ru, Co counterparts loadings and RuCo NPs were also prepared. The structure, morphology, size and composition of the catalysts with different metal NPs loadings were discussed in detail, and then investigated catalytic activity, durable stability of various catalysts and the influence factors. In addition, the activation energy (E_a) for the hydrolysis reaction has been measured by different temperature experiment.

2. Material and methods

2.1. Reagents and Chemicals

Aluminum nitrate nonahydrate, 1,3,5-benzenetricarboxylic acid (H_3btc), N,N-dimethylformamide (DMF), ruthenium chloride hydrate, cobalt chloride hexahydrate, sodium borohydride were purchased from Sinopharm Chemical Reagent Co., Ltd.. Ammonia borane (AB) was obtained from Energy Chemical. All chemicals employed were of analytical grade and used without further purification. Additionally, we used de-ionized water as the reaction solvent.

2.2. Synthesis of MIL-96(Al)

MIL-96(Al) was hydrothermally synthesized to follow the reported method [23]. Typically, H_3btc (208 mg), $Al(NO_3)_3 \cdot 9H_2O$ (460 mg) and de-ionized water (7 mL) were placed in a 40 mL Teflon-liner autoclave and heated at 210 °C for 12 h. After natural cooling, the suspension was filtered off to separate the white powder of

MIL-96(Al) with formula $\text{Al}_{12}\text{O}(\text{OH})_{18}(\text{H}_2\text{O})_3(\text{Al}_2(\text{OH})_4)[\text{btc}]_6 \cdot 24\text{H}_2\text{O}$ and then further purified by solvothermal treatment in DMF at 150 °C for 5 h. The separated resulting solid was refluxed overnight in a suspension of water at 100 °C for 12 h and immediately filtered. The resulting white solid was finally dried overnight in the vacuum oven at 80 °C for further use.

The structure description of MIL-96(Al) phase are learned from published papers [23], which exhibits a 3D framework resulting from the connection of aluminium octameric clusters linked through the trimesate (btc) ligand. An inorganic part consists of a 2D network containing chains of aluminum $\text{AlO}_2(\text{OH})_4$ and $\text{AlO}_4(\text{OH})_2$ octahedra, interconnected with each other to generate a hexagonal 18-membered ring in the (a, b) plane have been found in the MIL-96 framework (Fig. 1). The cohesion of the structure is ensured by the connection of the oxo-centered trinuclear aluminum units with the 2D network of aluminum octahedra through the trimesate molecules. The structure fully proves that MIL-96 has the characteristic of porous, which provides the possibility for the load of RuCo NPs.

2.3. Synthesis of $\text{Ru}_1\text{Co}_1@\text{MIL-96}$ and other catalysts

The $\text{Ru}_1\text{Co}_1@\text{MIL-96}$ catalyst was synthesized as follows: 200 mg of MIL-96 (Al) was added to a flask containing 30 mL of de-ionized water. Ultrasonication was required to get a uniform dispersion. Next, 10 mL RuCl_3 solution ($0.01 \text{ mol} \cdot \text{L}^{-1}$) and 10 mL $\text{CoCl}_2 \cdot 6\text{H}_2\text{O}$ solution ($0.01 \text{ mol} \cdot \text{L}^{-1}$) was added into the flask under magnetic stirring for 5 h. Then, 10 mL aqueous solution of NaBH_4 (50 mg) was added to this mixture and the resulting solution was stirred at room temperature for 5 h. The product was collected through filtration and dried in the vacuum oven at 80 °C for 12h to obtain the $\text{Ru}_1\text{Co}_1@\text{MIL-96}$ catalyst.

In order to compare the catalytic activity, the preparations of the $\text{Ru}_1\text{Co}_{0.5}@\text{MIL-96}$, $\text{Ru}_1\text{Co}_2@\text{MIL-96}$ and $\text{Ru}_1\text{Co}_3@\text{MIL-96}$ are following the above analogous process. During the synthesis of mono-metal $\text{Ru}@\text{MIL-96}$, $\text{Co}@\text{MIL-96}$ and pure RuCo NPs catalysts, the amounts of Ru and Co were consistent with that of $\text{Ru}_1\text{Co}_1@\text{MIL-96}$. In a typical synthesis of $\text{Co}@\text{MIL-96}$, 200 mg MIL-96 and 10 mL 0.01 mol

L^{-1} $\text{CoCl}_2 \cdot 6\text{H}_2\text{O}$ were diluted in 30 mL of de-ionized water. The solution was then introduced to a flask which contained 50 mg of NaBH_4 with vigorous stirring. And RuCo NPs was prepared as follows: 0.25 mL $0.01 \text{ mol} \cdot \text{L}^{-1}$ RuCl_3 and 0.25 mL $0.01 \text{ mol} \cdot \text{L}^{-1}$ CoCl_2 solution were added to a flask containing 30 mL of de-ionized water. Ultrasonication was required for 20 min to get a uniform dispersion, and then an aqueous solution of 10 mL $0.013 \text{ mol} \cdot \text{L}^{-1}$ NaBH_4 was added to this mixture followed by magnetic stirring for 5 h. The product was collected through filtration, washed with de-ionized water and ethanol for three times, and dried at 80°C overnight in a vacuum oven for further use.

2.4. Hydrolytic dehydrogenation of ammonia borane

The catalytic activity of RuCo@MIL-96 in the hydrolysis of AB was determined by measuring the rate of hydrogen generation. The experiment was conducted in a two-necked round bottom flask contain a mixture of 5 mg RuCo@MIL-96 and 10 mL de-ionized water. One neck was connected to a pressure-equalization funnel to introduce 10 mL aqueous solution of NH_3BH_3 (18.5 mg, 0.6 mmol) and the other neck was connected to a gas burette to monitor the volume of the gas evolution. The reaction started when the aqueous solution was added to the catalyst, and the volume of the generated hydrogen gas was recorded by the displacement level of water in the burette at a certain time interval (30 s). A water bath was used to control the reaction temperature at 25°C . In different Ru/Co molar ratio composites, 5 mg of Ru_1Co_x @MIL-96 ($x=0, 0.5, 1, 2, 3$) catalysts were employed for the hydrolysis of ammonia borane.

In order to get the activation energy (E_a) of the hydrolytic reaction, 18.5 mg AB was hydrolyzed with 5mg Ru_1Co_1 @MIL-96 at different temperatures (25, 30, 35 and 40°C).

The durability of Ru_1Co_1 @MIL-96 catalyst in the hydrolysis of AB was evaluated by performing the recyclability tests at room temperature. In a typical test, 10 mL of Ru_1Co_1 @MIL-96 (5 mg) suspension solution and 18.5 mg AB (10 ml, 0.6 mmol) were added into the reaction flask at 25°C , and the evolution of gas was

measured as described above. After the hydrolysis reaction was completed, another equivalent of AB (18.5mg) was subsequently added into the reaction flask. The evolution of gas was monitored by using the gas burette. The tests were repeated five times at room temperature. After the tests, the catalysts were separated from the reaction solution by centrifugation and washed with water for several times and dried in the vacuum oven at 80 °C.

In a typical reusability test, 18.5 mg AB (10 mL, 0.6 mmol) was added to 10 mL of Ru₁Co₁@MIL-96 (5 mg) suspension solution, the evolution of gas was monitored as described above. After the hydrolysis reaction was completed, the Ru₁Co₁@MIL-96 catalyst was isolated and redispersed in 10 mL de-ionized water. Then, 18.5 mg AB (10 mL, 0.6 mmol) was added into the reaction flask for a subsequently run of hydrolysis at 25 °C.

The maximum productivity of Ru₁Co₁@MIL-96 catalyst in the hydrolysis of AB was determined by measuring the turnover number (TON, moles of H₂/moles of catalyst). In a typical test, 10 mL of Ru₁Co₁@MIL-96 (5 mg) suspension solution and 10 mL AB (18.5 mg) were added into the reaction flask at 25 °C, and the evolution of gas was measured as described above. Once complete conversion is achieved, another equivalent of AB was added and the reaction was continued until no hydrogen gas evolution was observed.

2.5. Catalyst characterization

The morphologies and composition of the samples were observed by using a Tecnai G20 U-Twin transmission electron microscope (TEM) equipped with an energy dispersive X-ray detector (EDX) at an acceleration voltage of 200 kV. Powder X-ray diffraction (XRD) patterns were measured by a Bruker D8-Advance X-ray diffractometer using Cu K α radiation source ($\lambda=0.154178$ nm) with a velocity of 10° min⁻¹ to identify the phase purity and crystallinity. Fourier transform infrared (FT-IR) spectroscopic experiment was carried out on a Nicolet (Madison, WI, USA) Impact 420 apparatus to determine the structure of MIL-96. The electronic states of the as-synthesized samples were investigated by X-ray photoelectron spectroscopy (XPS,

Thermo ESCALAB 250Xi). The metal loadings of catalysts were determined by an IRIS Intrepid IIXSP inductively coupling plasma-atomic emission spectrometer (ICP-AES). The surface area measurements were performed with N₂ adsorption-desorption isotherms obtained at 77 K using a Micromeritics ASAP 2020 instrument.

3. Results and discussion

The XRD patterns of the as-prepared MIL-96, Ru@MIL-96, Co@MIL-96, Ru₁Co₁@MIL-96 and Ru₁Co₁@MIL-96 after the fifth run catalysts are illustrated in Fig. 2A, respectively. It can be seen that the XRD pattern of MIL-96 is in good agreement with the previously reported one [23], confirming that MIL-96 is successfully synthesized. The patterns of Ru@ MIL-96, Co@MIL-96 and Ru₁Co₁@MIL-96 samples are matched with those of the host MIL-96, indicating that the integrity of the MIL-96 framework is maintained well during the catalyst preparation and catalytic process. However, the decrease in intensity of peaks as compared with MIL-96 can be explained by the changes in the charge distribution and electrostatic fields as a result of the existence of RuCo NPs on the surface and interaction of their electrophilic surface with framework atoms [24]. Additionally, the diffraction peaks corresponding to the Ru and/or Co NPs were indicated in Fig. 2B, the weak intensities were probably as a result of low metal loading or the amorphous phases of Ru and Co NPs [25]. Moreover, Fig.2C shows the diffraction peaks of Ru at around 44.1° in the Ru@MIL-96 catalyst. However, the peak of Ru shifts slightly to higher 2θ values from 44.1° to 44.7° in Ru₁Co₁@MIL-96 compared to Ru@MIL-96, that indicates the incorporation of small Co atoms into Ru lattice results in a lattice contraction [26]. The above results show that RuCo alloys are formed in Ru₁Co₁@MIL-96 catalyst rather than a physical mixture of individual metal NPs [27]. Based on the formation of RuCo alloy NPs, positive synergistic effect among noble metal Ru and non-noble metal Co could be achieved, that leads to the highly catalytic activity for catalytic hydrolysis of AB.

The X-ray photoelectron spectroscopy (XPS) was employed to demonstrate metallic electronic states in the Ru₁Co₁@MIL-96 catalyst. Fig. 3a shows the survey

scan X-ray photoelectron spectra of as-prepared Ru₁Co₁@MIL-96 catalyst. It can be seen that the main absorptions belong to C 1s, Ru 3d, Ru 3p, Co 2p, and O 1s. Due to the strong overlap of the C 1s and Ru 3d peaks around 284.7 eV, it is very difficult to analyze this region for ruthenium properly. Fig. 3b shows the absorptions located at 462.0 and 485.1 eV for Ru 3p_{3/2} and Ru 3p_{1/2}, respectively, are readily assigned to the Ru(0) [28]. In Fig. 3c, the peak of Co 2p reveals four peaks at 797.8 and 803.6 eV for Co(II) 2p_{1/2}, 781.6 and 786.3 eV for Co(II) 2p_{3/2} [29-31]. The two weak peaks at 777.9 and 793.0 eV are attributed to Co(0) 2p_{3/2} and Co(0) 2p_{1/2} [22]. These results indicate that Ru is stable in the catalyst, whereas Co may be oxidized to certain degree during the synthesis of the Ru₁Co₁@MIL-96 catalyst.

The morphologies, particles dispersed state and element composition of RuCo NPs loaded on MIL-96 were further characterized by TEM and EDX techniques. Fig. 4 shows the TEM images of the as-synthesized (a,b) and used (c,d) Ru₁Co₁@MIL-96, in which the lattice fringes can be clearly observed and there are many small particles loaded on the crystal surface. Fig. 4a, c and Fig. 4b, d are the low and high resolution TEM images of the Ru₁Co₁@MIL-96 sample, respectively. From Fig. 4a,b, it can be seen that the MIL-96 displays a nanofibrous morphology with a width of 5~10 nm and length of 100~200 nm, and most RuCo NPs with a narrow particle size distribution are uniformly dispersed on the surface of MIL-96. Particle size distribution of Ru@MIL-96 and Co@MIL-96 were shown in Fig. 4g,h, it can be seen that the mean particle diameter of Ru in the Ru@MIL-96 and Co in Co@MIL-96 were about 2.3±0.3nm and 6.7±0.3nm, respectively. The mean particle diameter of RuCo particles of as-prepared Ru₁Co₁@ MIL-96 was about 1.7 nm (Fig. 4e), and the standard deviation was determined to be 0.3nm, while the diameter of pore of the support MIL-96 was about 1.66 nm, resulting in most of RuCo NPs locate at the external surface of the crystal. However, it could not preclude that there are still some smaller RuCo NPs (<1.66 nm) embedded within the frameworks, these NPs difficult to be identified by TEM imaging. And no significant aggregate is formed, which is the basis for high performance of the catalyst, probably because the MIL-96 structures offer steric restrictions that strengthen the synergistic reaction between Co and Ru

NPs on the surface of MIL-96. In Fig. 4(c,d), after five catalytic cycles, it can be seen that the Ru₁Co₁@MIL-96 catalyst still remains the structure of the MIL-96 and shows an excellent stability, and a number of NPs are well dispersed on the surface of MIL-96. The particle size distribution of the Ru₁Co₁@MIL-96 catalyst after the fifth run was shown in Fig. 4i, the mean particle diameter and the standard deviation of RuCo particles of was about 1.9±0.3nm. From Fig. 4i, the particle size distribution of Ru₁Co₁@MIL-96 after the fifth run almost keeps unchanged compared with that of the as-prepared Ru₁Co₁@MIL-96. In order to further confirm the presence of RuCo NPs, the EDX spectrum was measured, see Fig. 4f. Moreover, the actual RuCo loading effect and ratio of the metals Ru, Co in RuCo@MIL-96 catalysts were measured by ICP-AES, as shown in Table 1. The results show that the actual ratios of Ru:Co is almost similar to the precursor ratios 1:0,1:0.5,1:1,1:2,1:3 in the Ru₁Co_x@MIL-96 (x=0,0.5,1,2,3) catalysts. And the Co contents are obviously lower than its initial additive amount in all samples. This is probably because Ru³⁺ can be readily reduced to Ru by NaBH₄, but it is difficult to reduce Co²⁺ to Co due to the lower reduction potentials of Co²⁺/Co (reduction potentials: E^θ(Ru³⁺/Ru)=+0.40 eV; E^θ(Co²⁺/Co)= -0.28 eV). In the Ru₁Co₁@ MIL-96 catalyst, the actual loadings of Ru and Co are 2.07 and 1.19 wt%, respectively.

From Fig. 5(a,b), the specific surface areas estimated from the N₂ adsorption-desorption isotherms of MIL-96(Al) support and the as-prepared Ru₁Co₁@MIL-96(Al) were 443.6 m²/g and 205.4 m²/g, respectively, further confirming the highly porous structure of MIL-96 support. Resulted from the porous structure, the surface area of MIL-96(Al) is much higher than that of Ru₁Co₁@MIL-96, the significant decrease in the surface area of Ru₁Co₁@MIL-96 indicates that the cavities of MIL-96(Al) are either occupied or blocked by the well-dispersed RuCo NPs. Fig. 5(c) shows the pore size of MIL-96 and Ru₁Co₁@MIL-96. The pore volume of MIL-96 was determined to be 0.094 cm³ g⁻¹, and its pore size was calculated to be 1.66 nm. However, after the loading of RuCo NPs, the pore volume of MIL-96 decreased to 0.051 cm³ g⁻¹, and the corresponding pore size from 1.66 to 1.08 nm. The reason for this phenomenon is that the relatively small size RuCo alloy NPs occupied or blocked the cavities of MIL-96

and the big size alloy NPs mainly deposited on the surface of MIL-96, that directly lead to a decrease in the pore volume and pore size.

The functional groups of MIL-96 and MIL-96 supported RuCo NPs were investigated by FT-IR, as shown in Fig. 6. It can be seen that the intensity and position of FT-IR peaks of Ru₁Co₁@MIL-96 after the fifth run show no obvious change compared to that of MIL-96 and initial Ru₁Co₁@MIL-96 catalyst, indicating that the crystalline structure of the host of MIL-96 is unchanged, that provides favorable conditions for RuCo NPs effectively immobilized in the framework of MIL-96 after the catalytic cycles.

The catalytic properties of the as-obtained Ru@MIL-96, Co@MIL-96 and Ru₁Co₁@MIL-96 samples were systematically evaluated in the catalytic hydrogenation of AB at room temperature. Fig. 7 shows that the Ru₁Co₁@MIL-96 exhibits the highest activity compared with monometallic Ru@MIL-96 and Co@MIL-96. Furthermore, the same amount of RuCo NPs reduced by NaBH₄ without the support MIL-96(Al) also is applied to hydrolysis of AB, only 31 mL H₂ were released for more than 15 min, and MIL-96 almost no activity. Reasonably, the Ru₁Co₁@MIL-96 remarkably high catalytic activity is first attributed to the synergetic effect between Ru and Co alloy NPs. For alloy NPs, synergetic effects may be mainly ascribed to electronic effects, which are important when the metal atoms have significant differences in electronegativity [32], and geometric effects. In the present case, the observed synergetic effects in catalysis might be mainly due to the electronic effects, not the geometric effects, because the disparity of electronegativity, Ru (2.3) and Co(1.88), is prominent. Additionally, the bi-functional effects between RuCo alloy NPs and MIL-96 are significantly enhanced the reaction activity of Ru₁Co₁@MIL-96 catalyst, in which MIL-96 can provide a good 3D framework for RuCo NPs in spite of it does not involved in the hydrolysis reaction of AB. By calculating, the turn over frequency (TOF) value of Ru₁Co₁@MIL-96 is determined to be 320.7 mol H₂ min⁻¹ (mol Ru)⁻¹, which is higher than most Ru-based catalysts ever reported for the catalytic hydrolysis of AB (Table 2).

For a comprehensive elucidation of the catalytic activity of the RuCo@MIL-96

catalytic architecture towards hydrolytic dehydrogenation of AB, we followed a systematic approach, where the single-component samples Ru@MIL-96 and Co@MIL-96 catalytic performance were studied in addition to binary combinations of these subcomponents, namely Ru₁Co_{0.5}@MIL-96, Ru₁Co₁@MIL-96, Ru₁Co₂@MIL-96 and Ru₁Co₃@MIL-96 (Fig. 8a). Evidently, Ru₁Co₁@MIL-96 catalyst provides the highest activity compared to all other investigated catalysts. By changing the molar ratio of Ru to Co, the reaction rate increased at first and then decreases, as shown in Fig. 8b. The observed “volcano”- type activity of the RuCo@MIL-96 catalysts versus Ru/Co molar indicates that neither Ru nor Co has enough activity for catalyzing the hydrolytic dehydrogenation of AB at complete conversion. This phenomenon may be relevant to catalytic mechanism of the RuCo@MIL-96 catalysts for the hydrolysis reaction of AB. To the best of our knowledge, the heterogeneous catalytic reaction takes place on the surface area of the metal catalyst [45]. The mechanism involves two steps. Firstly, AB interacts with the surface of RuCo alloy NPs to form the activated transient Metal-H, which is the prerequisite for the hydrolysis reaction. Then, H₂ was released after the attack of water on the Metal-H species [46,47]. With the increasing loading of Co, and RuCo alloy NPs were uniformly dispersed on the surface of the MIL-96, that caused an increase in the contact area between metal NPs and AB as well as the number of active sites with the activated transient Metal-H. Therefore, based on the increasing contact area, the activated transient Metal-H and the synergistic catalysis effect of alloying Ru with Co in the RuCo@MIL-96 catalyst, the catalytic activity obviously enhanced with the increase Ru:Co ratio 1:0.5,1:1. However, more Co loading would result in the excess coverage of Ru active sites [48], or the reactant bound to the catalyst surface too strongly, that would occupy all available surface sites and poison the catalyst [49], causing the lower activity for hydrogen generation from the hydrolysis of AB.

In comparison with the case of the monometallic Ru@MIL-96 and Co@MIL-96 catalyst, all the hydrogen generation rate and productivity were recorded in Fig.8c, it is obvious that Co@MIL-96 almost have no catalytic activity toward hydrolysis of AB, and with the same amount of Ru, monometallic catalyst Ru@MIL-96 has much

inferior catalytic activity than that of Ru₁Co₁@MIL-96. As can be seen from Fig. 8d, when the molar ratio of Ru to Co contained the same as that of Ru₁Co₁@MIL-96, the catalytic performance of the mixture of monometallic counterparts Ru@MIL-96 and Co@MIL-96 is obviously inferior to that of the Ru₁Co₁@MIL-96 catalyst. The result fully confirms the strong synergistic effects among noble metal Ru and non-noble metal Co. Moreover, the catalytic activity of Ru₁Co₁@MIL-96 is superior to that of pure RuCo NPs, which demonstrates the bi-functional effects between RuCo alloy NPs and the host of MIL-96 in the process of hydrolysis of AB.

In order to get the activation energy (E_a) of the AB hydrolysis catalyzed by Ru₁Co₁@MIL-96, the hydrolytic experiments at different temperatures ranged from 25 to 40 °C were carried out. Fig. 9a shows that the hydrolytic rates increase with the increase of reaction temperature, and the values of rate constant k at different temperature are calculated from the slope of the linear part of each plot. The Arrhenius plot of lnk vs. 1/T for the catalyst is plotted in Fig. 9b, from which the apparent activation energy (E_a) is determined to be approximately 36.0 kJ/mol for AB. Although this value is higher than that reported for several Ru-based catalysts (Table 2), it is lower than most of the reported activation energy values for the same reaction using many different catalysts even with some noble-metal containing catalysts, indicating that the as-obtained Ru₁Co₁@MIL-96 catalyst is very promising candidates for the hydrolysis of AB.

The durability research is the key point for the practical application of catalysts. Fig. 10a shows that the Ru₁Co₁@MIL-96 catalyst still exhibits excellent catalytic activity after multiple cycles of reaction. Fig. 10b shows the conversion of AB and the retained percent catalytic activity in the subsequent catalytic runs for the hydrolysis of AB. The as-synthesized Ru₁Co₁@MIL-96 catalyst retains about 90.5% of its initial catalytic activity toward hydrolysis of AB after the second run and the following three times are 83.6%, 75.7% and 69.7%, respectively. The metal leaching in different uses were determined to be 6.30%, 9.99%, 12.44%, 14.34% and 16.02%, respectively (Table 3). The high durability of the catalyst should be attributed to the fact that the crystalline structure of the catalyst is mostly unchanged and the ultrafine RuCo alloy

NPs still have been effectively immobilized in the framework of MIL-96 through the catalytic cycles. The representative TEM image of Ru₁Co₁@ MIL-96 catalyst after the fifth durability test is shown in Fig. 4c,d. There is no obvious change in the morphology of the catalyst and metal NPs still have good load, confirming that MIL-96 can stabilize RuCo NPs for good durability and confinement effect. Therefore, the decrease of the catalytic activity might be caused by the increasing viscosity of the reaction solution and/or the deactivation effect of the increasing metaborate concentration during the hydrolysis of AB as well as the Ru and Co metal leaching [18,50]. From Fig. 10c, it can be seen that Ru₁Co₁@MIL-96 also shows high reusability during five runs. The life-time of the catalyst in the AB hydrolysis was determined by calculating the TON, in which the molar ratio of ammonia borane vs catalyst was controlled more than 50,000. Fig. 10(d) shows the variation of TON versus time during the hydrolysis of AB, from which we can see that the Ru₁Co₁@MIL-96 catalyst has 30400 turnovers in the hydrolysis of AB at 25°C before deactivated. Based on the observations above, the Ru₁Co₁@MIL-96 catalyst is highly stable toward the hydrolytic dehydrogenation of AB.

4. Conclusion

In summary, the RuCo alloy NPs supported on MIL-96 have been designed and successfully prepared. The obtained Ru₁Co₁@MIL-96 nanocatalysts exhibit excellent catalytic activity and durability for hydrolytic dehydrogenation of aqueous AB at room temperature, owing to its strong bimetallic synergistic effects, uniform dispersion of NPs on the surface of MIL-96 and bi-functional effects between RuCo alloy NPs and the host of MIL-96. The activation energy (E_a) and turn over frequency (TOF) are determined to be 36.0 kJ/mol and 320.7 mol H₂ min⁻¹(mol Ru)⁻¹, respectively. In addition, this simple synthetic method can be easily extended to facile preparation other MOFs supported metal NPs. Moreover, more non-noble metal component in the catalyst not only improves the catalytic activity, but also reduces the cost which is the key to building a sustainable development of industry in the future. The superior catalytic performance of the RuCo@MIL-96 makes it an ideal catalyst

for hydrolysis of AB using as a highly efficient portable hydrogen storage material.

Acknowledgments

This project was supported by the Natural Science Fund for Creative Research Groups of Hubei Province (2014CFA015) of China. This work was also supported by the Hubei College Students' Innovation Training Program of China (201410512024, 201510512030).

References

- [1] A. F. Dalebrook, W. Gan, M. Grasmann, *Chem. Commun.* 49 (2013) 8735.
- [2] G. W. Crabtree, M. S. Dresselhaus, M. V. Buchanan, *Phys. Today* 57 (2004) 39.
- [3] J. Graetz, *Chem. Soc. Rev.* 38 (2009) 73.
- [4] M. P. Suh, H. J. Park, T. K. Prasad, *Chem. Rev.* 112 (2011) 782.
- [5] A. Staubitz, A. P. M. Robertson, I. Manners, *Chem. Rev.* 110 (2010) 4079.
- [6] A. D. Sutton, A. K. Burrell, D. A. Dixon, *Science* 331 (2011) 1426.
- [7] M. Ramzan, F. Silvearv, A. Blomqvist, *Phys. Rev. B* 79 (2009) 132102.
- [8] C. W. Hamilton, R. T. Baker, A. Staubitz, *Chem. Soc. Rev.* 38 (2009) 279.
- [9] D. Sun, V. Mazumder, O. Metin, *ACS Catal.* 2 (2012) 1290.
- [10] J. Zhang, C. Chen, W. Yan, *Catal. Sci. Technol.* 6 (2016) 2112.
- [11] S. Akbayrak, S. Özkar, *Dalton Trans.* 43 (2014) 1797.
- [12] J. Yang, E. Sargent, S. Kelley, *Nat. Mater.* 8 (2009) 683.
- [13] X. Xiong, L. Zhou, G. Yu, *Int. J. Hydrogen Energy* 40 (2015) 15521.
- [14] K. Yang, L. Zhou, X. Xiong, *Microporous Mesoporous Mater.* 225 (2016) 1.
- [15] H. Furukawa, K. E. Cordova, M. O'Keeffe, *Science* 341 (2013) 1230444.
- [16] C. Wang, D. Liu, W. Lin, *J. Am. Chem. Soc.* 135 (2013) 13222.
- [17] D. Bradshaw, A. Garai, J. Huo, *Chem. Soc. Rev.* 41 (2012) 2344.
- [18] N. Cao, T. Liu, J. Su, *New J. Chem.* 38 (2014) 4032.
- [19] H. Dai, J. Su, K. Hu, *Int. J. Hydrogen Energy* 39 (2014) 4947.
- [20] L. Wen, J. Su, X. Wu, *Int. J. Hydrogen Energy* 39 (2014) 17129.
- [21] B. Xia, C. Liu, H. Wu, *Int. J. Hydrogen Energy* 40 (2015) 16391.
- [22] J. Li, Q. L. Zhu, Q. Xu, *Catal. Sci. Technol.* 5 (2015) 525.
- [23] T. Loiseau, L. Lecroq, C. Volkringer, *J. Am. Chem. Soc.* 128 (2006) 10223.
- [24] M. Yurderi, A. Bulut, M. Zahmakiran, *Appl. Catal. B* 160 (2014) 534.
- [25] M. S. El-Shall, V. Abdelsayed and S. K. Abd El Rahman, *J. Mater. Chem.* 19 (2009) 7625.
- [26] J. Cai, Y. Huang, Y. Guo, *Appl. Catal. B* 150 (2014) 230.
- [27] D. Liang, J. Gao, J. Wang, *Catal. Commun.* 12 (2011) 1059.
- [28] M. N. Timofeeva, V. N. Panchenko, A. A. Abel, *J. Catal.* 311 (2014) 114.
- [29] M. Rakap, *J. Alloys Compd.* 649 (2015) 1025.
- [30] X. Li, C. Zeng, G. Fan, *Int. J. Hydrogen Energy* 40 (2015) 9217.
- [31] E. Meza, J. Ortiz, D. Ruíz-León, *Mater. Lett.* 70 (2012) 189.

- [32] L. Yang, J. Su, X. Meng, *J. Mater. Chem. A* 1 (2013) 10016.
- [33] H. Liang, G. Chen, S. Desinan, *Int. J. Hydrogen Energy* 37 (2012) 17921.
- [34] J. Wang, Y. L. Qin, X. Liu, *J. Mater. Chem.* 22 (2012) 12468.
- [35] N. Cao, J. Su, W. Luo, *Int. J. Hydrogen Energy* 39 (2014) 426.
- [36] S. Akbayrak, S. Özkar, *ACS Appl. Mater. Interfaces* 4 (2012) 6302.
- [37] S. Akbayrak, S. Tanyıldızı, İ. Morkan, *Int. J. Hydrogen Energy* 39 (2014) 9628.
- [38] N. Cao, K. Hu, W. Luo, *J. Alloys Compd.* 590 (2014) 241.
- [39] Q. Xu and M. Chandra, *J. Alloys Compd.* 446 (2007) 729.
- [40] L. Hu, B. Zheng, Z. Lai, *Int. J. Hydrogen Energy* 39 (2014) 20031.
- [41] H. Can and Ö. Metin, *Appl. Catal. B* 125 (2012) 304.
- [42] M. Chandra, Q. Xu, *J. Power Sources* 168 (2007) 135.
- [43] J. Liao, H. Li, X. Zhang, *Catal. Sci. Technol.* 6 (2016) 3893.
- [44] K. Güngörmez, Ö. Metin, *Appl. Catal. A* 494 (2015) 22.
- [45] D. Ke, Y. Li, J. Wang, *Int. J. Hydrogen Energy* 41 (2016) 2564.
- [46] Q. Xu, M. Chandra, *J. Power Sources* 163 (2006) 364.
- [47] G. Guella, C. Zanchetta, B. Patton, *J. Phys. Chem. B* 110 (2006) 17024.
- [48] Y. Huang, J. Cai, Y. Guo, *Appl. Catal. B* 129 (2013) 549.
- [49] Y. Li, Y. Dai, X. Tian, *Int. J. Hydrogen Energy* 40 (2015) 9235.
- [50] M. Rakap, S. Özkar, *Int. J. Hydrogen Energy* 35 (2010) 3341.

Table 1 - Elemental analysis of Ru₁Co_x@MIL-96 catalysts determined by ICP-AES.

Table 2 - Various catalyst systems tested in the hydrolysis of ammonia borane at room temperature.

Table 3 - The metal leaching of Ru₁Co₁@MIL-96 (5 mg) in the subsequent runs of the hydrolysis of ammonia borane.

ACCEPTED MANUSCRIPT

catalysts	Ru_1Co_0	$\text{Ru}_1\text{Co}_{0.5}$	Ru_1Co_1	Ru_1Co_2	Ru_1Co_3
Precursor ratios Ru:Co	1:0	1:0.5	1:1	1:2	1:3
Actual ratios Ru:Co	1:0	1:0.47	1:0.99	1:1.93	1:2.78
Actual loading of Ru wt%	1.88	1.99	2.07	2.05	1.91
Actual loading of Co wt%	0	0.55	1.19	2.31	3.09

Table 1

Catalyst	Ru/AB or Metal/AB(mol/mol)	TOF ^a (mol H ₂ mol ⁻¹ M min ⁻¹)	E _a (kJ mol ⁻¹)	Ref.
Ru/C	0.004(Ru/AB)	429.5	34.81	[33]
Pd@Co/graphene	0.02(Metal/AB)	408.9	-	[34]
Ru@Ni/graphene	0.004(Ru/AB)	339.5	36.59	[35]
Ru(0)@MWCNTs	0.0019(Ru/AB)	329	33	[36]
RuCo@MIL-96	0.0017(Ru/AB)	320.7	36.0	This study
Ru(0)/TiO ₂	0.005(Ru/AB)	241	70	[37]
RuCu/graphene	0.004(Ru/AB)	135	30.39	[38]
2 wt.% Pt/C	0.018(Metal/AB)	111	-	[39]
NiAgPd/C	0.012(Metal/AB)	93.8	38.36	[40]
Ru@Al ₂ O ₃	0.005(Ru/AB)	83.3	48	[41]
Ru/γ-Al ₂ O ₃	0.009(Ru/AB)	77	23	[42]
NiCo ₂ O ₄	0.0083(Metal/AB)	50.1	17.5	[43]
Cu ₇₅ Pd ₂₅ /RGO	0.003(Metal/AB)	29.9	45.9	[44]
Pt black	0.018(Metal/AB)	13.89	-	[39]

^aTOF values were taken directly from the related articles if they were reported. If not, the initial TOF values were calculated from the corresponding hydrogen generation versus time graphs presented in the article.

Table 2

Run	Ru leaching (mg)	Co leaching (mg)	Metal leaching (%)
1	0.0060	0.0043	6.30
2	0.0102	0.0061	9.99
3	0.0131	0.0072	12.44
4	0.0155	0.0079	14.34
5	0.0176	0.0085	16.02

Table 3

Figure captions:

Fig. 1. View of the corrugated chains in MIL-96.

Fig. 2. Low-angle (A), wide-angle (B) and the magnified Ru (C) powder XRD patterns of samples: (a) MIL-96; (b) Ru@MIL-96; (c) Co@MIL-96; (d) Ru₁Co₁@MIL-96; (e) Ru₁Co₁@MIL-96 after the fifth run.

Fig. 3. XPS spectra of Ru₁Co₁@MIL-96: (a) as-prepared; (b) Ru 3p; (c) Co 2p.

Fig. 4. TEM images of (a-b) as-prepared Ru₁Co₁@MIL-96; (c-d) Ru₁Co₁@MIL-96 after the fifth run; particle size distribution of (e) as-prepared Ru₁Co₁@MIL-96; (f) EDX spectrum of Ru₁Co₁@MIL-96; particle size distribution of (g) Ru@MIL-96; (h) Co@MIL-96; (i) Ru₁Co₁@MIL-96 after the fifth run.

Fig. 5. N₂ sorption isotherms of (a) MIL-96 and (b) as-prepared Ru₁Co₁@MIL-96; (c) pore size distribution of MIL-96 and Ru₁Co₁@MIL-96.

Fig. 6. FT-IR of (a) MIL-96; (b) initial Ru₁Co₁@MIL-96; (c) Ru₁Co₁@MIL-96 after the fifth run.

Fig. 7. Hydrogen generation from the hydrolysis of AB catalyzed by MIL-96, Ru@MIL-96, Co@MIL-96, Ru₁Co₁@MIL-96 and RuCo NPs (5mg catalysts, 18.5mg AB at 25 °C).

Fig. 8. (a) Hydrogen generation rate from the hydrolysis of AB catalyzed by different Ru, Co based catalysts; (b) the plot of hydrogen generation rate versus Co molar ratio for the hydrolytic dehydrogenation of AB; (c) hydrogen generation rate from the hydrolysis of AB catalyzed by Ru@MIL-96, Co@MIL-96 and Ru₁Co₁@MIL-96; (d) hydrogen generation rate from the hydrolysis of AB in the presence of Ru₁Co₁@MIL-96, RuCo NPs or the physical mixture of Ru@MIL-96+Co@MIL-96 (5mg catalysts, 18.5mg AB at 25 °C).

Fig. 9. (a) Temperature effects on hydrogen generation rate catalyzed by Ru₁Co₁@MIL-96 from AB hydrolysis (5mg catalysts, 18.5mg AB) in the range of 25-40 °C and (b) Arrhenius plot obtained from temperature effects.

Fig. 10. (a) Durability of the Ru₁Co₁@MIL-96 catalyst from 1st to 5th cycles; (b) percentage of initial catalytic activity of Ru₁Co₁@MIL-96 in successive runs for the hydrolysis of AB; (c) The plot of mol H₂ per mol AB versus time for hydrolysis of AB in the presence of Ru₁Co₁@MIL-96 during a five-cycle reusability test; (5mg catalysts, 18.5mg AB at 25 °C) (d) The turnover number (TON) versus time plot for Ru₁Co₁@MIL-96.

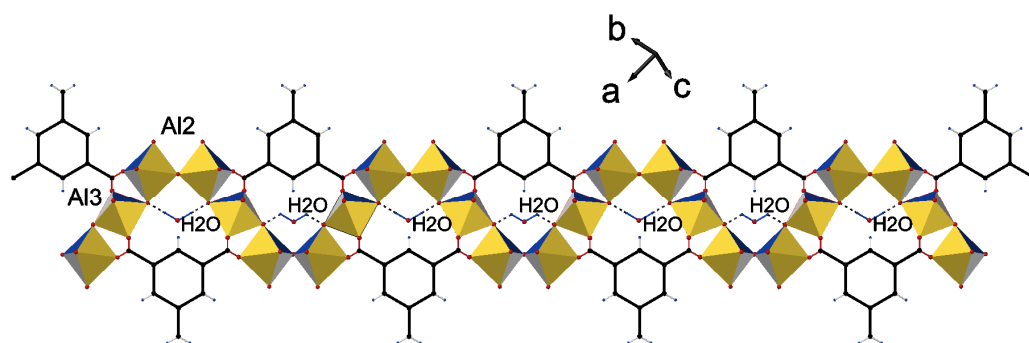
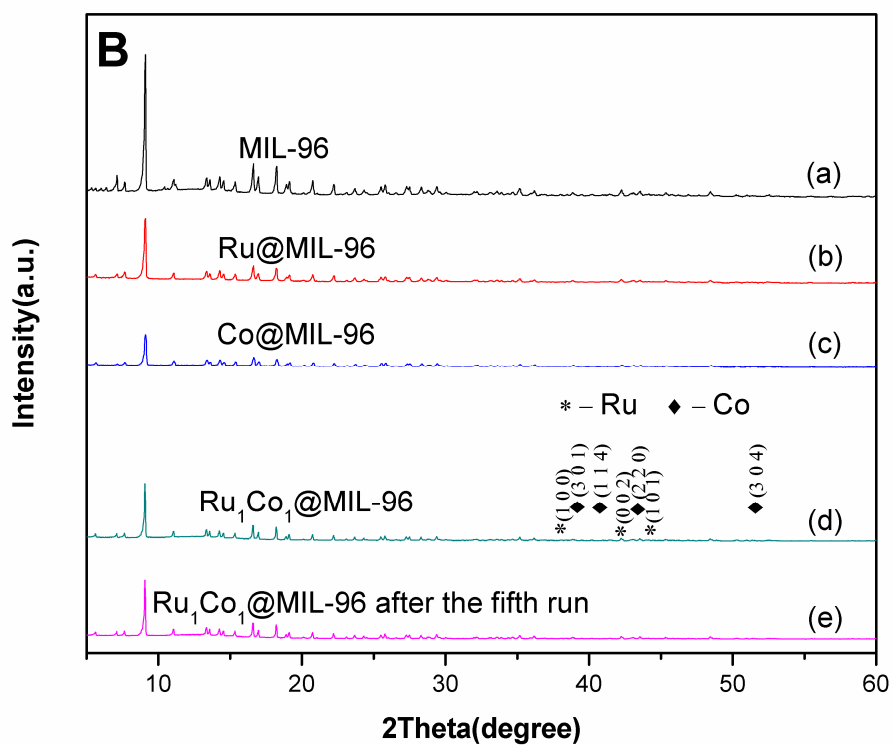
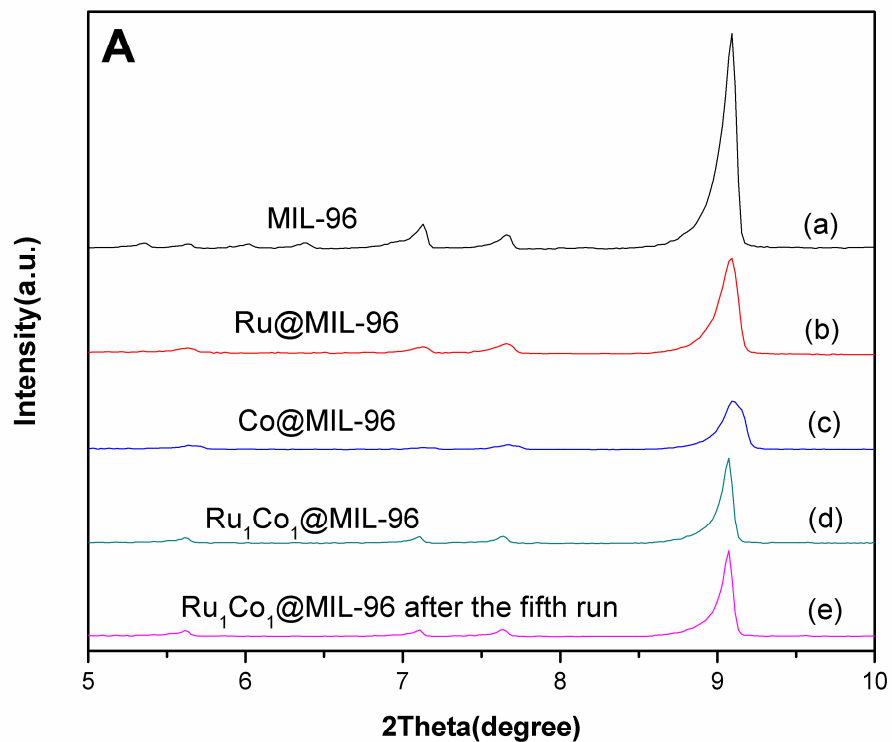


Fig. 1



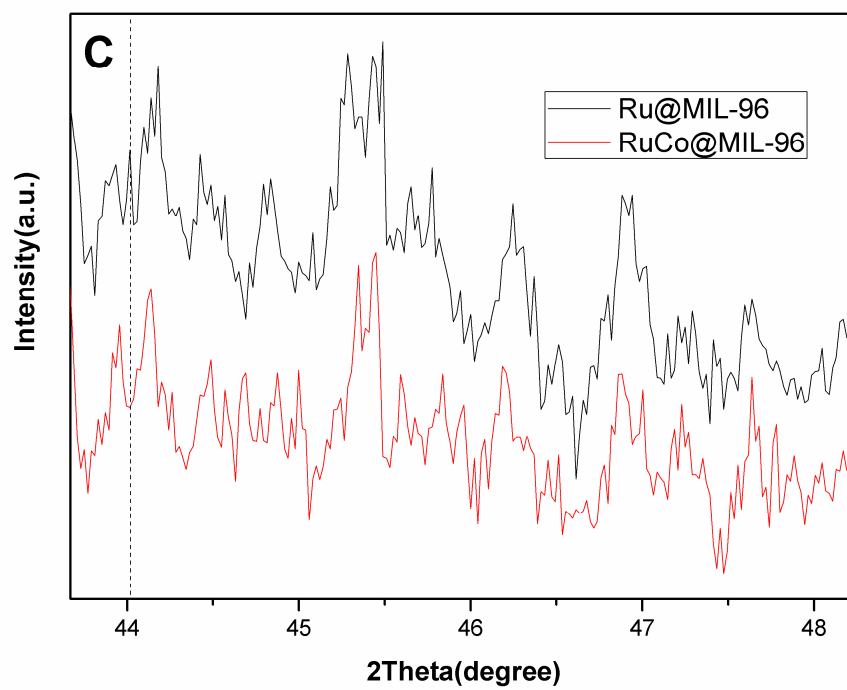
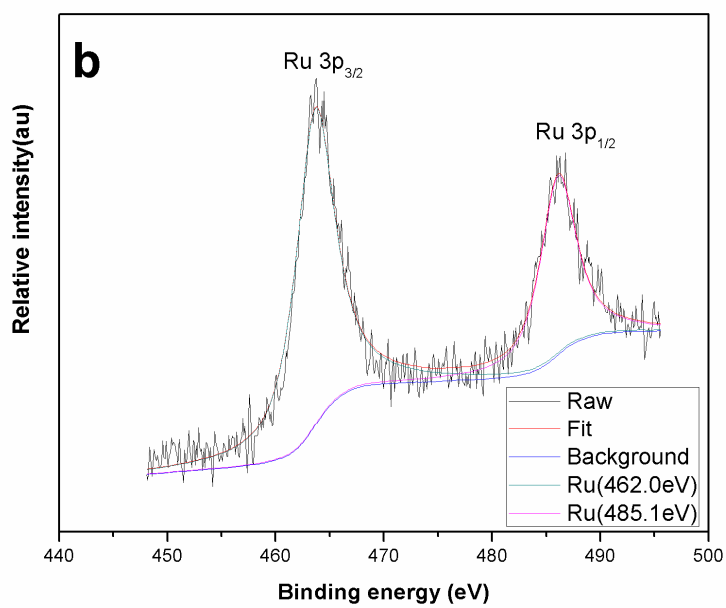
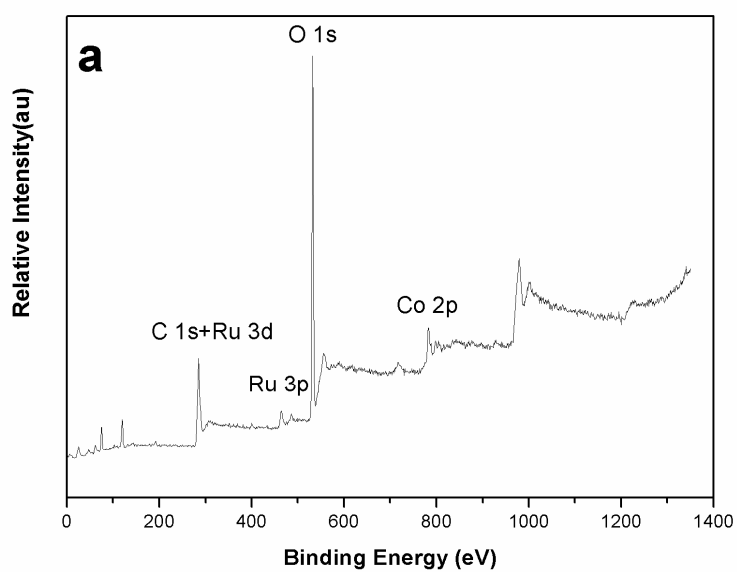


Fig. 2



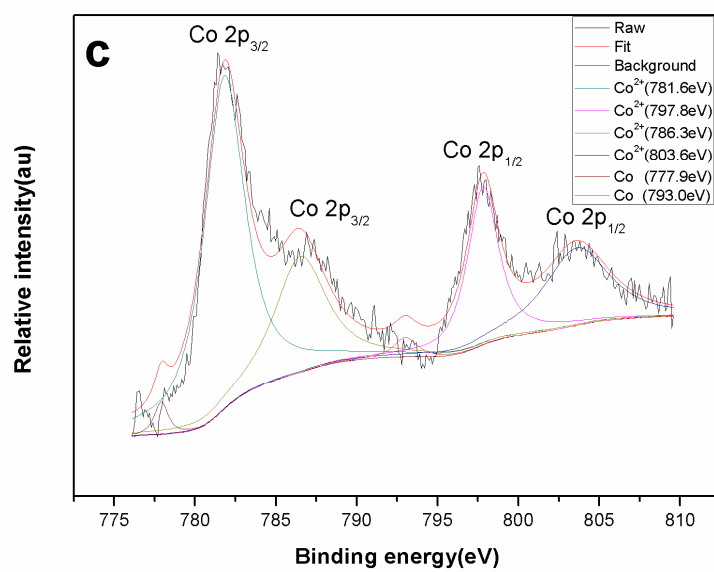
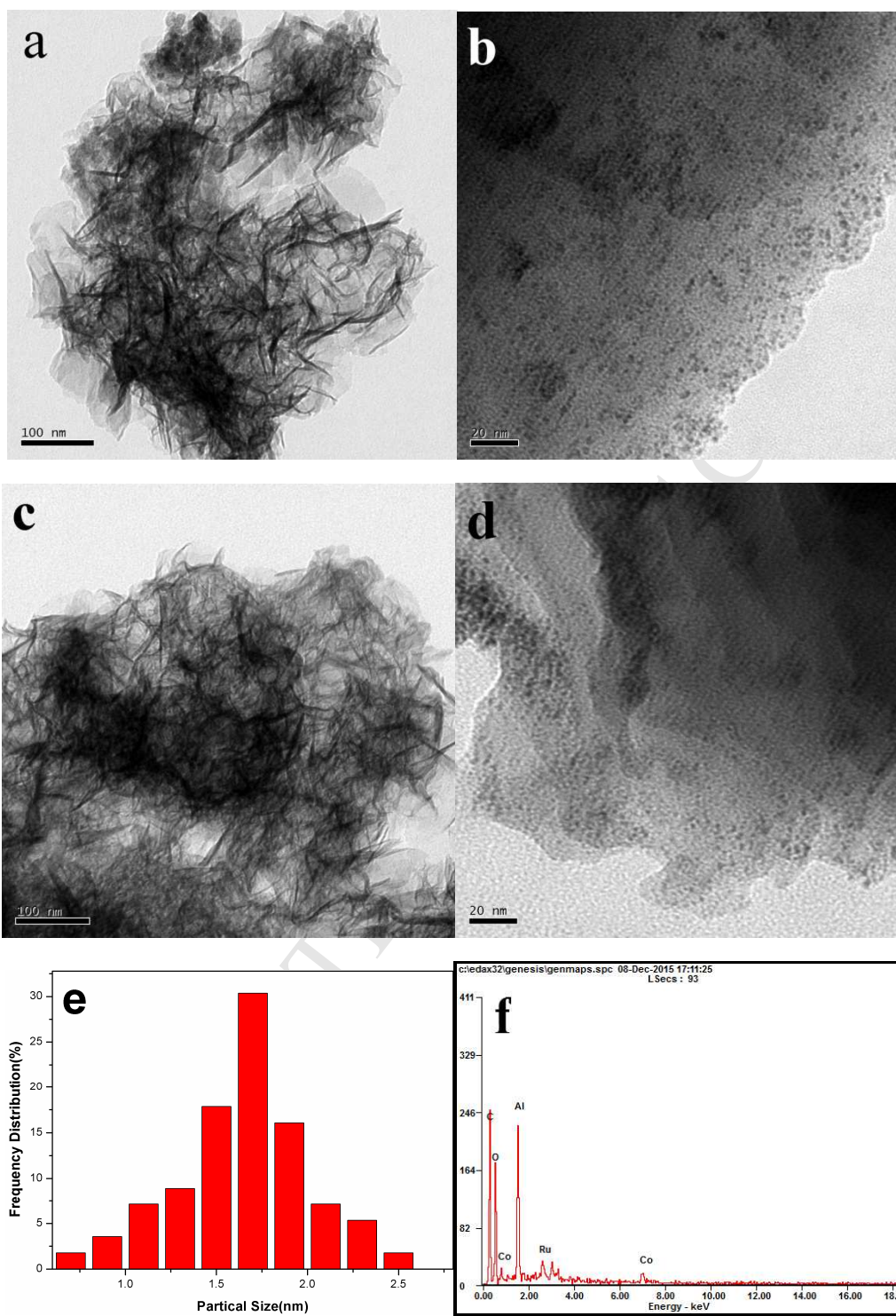


Fig. 3



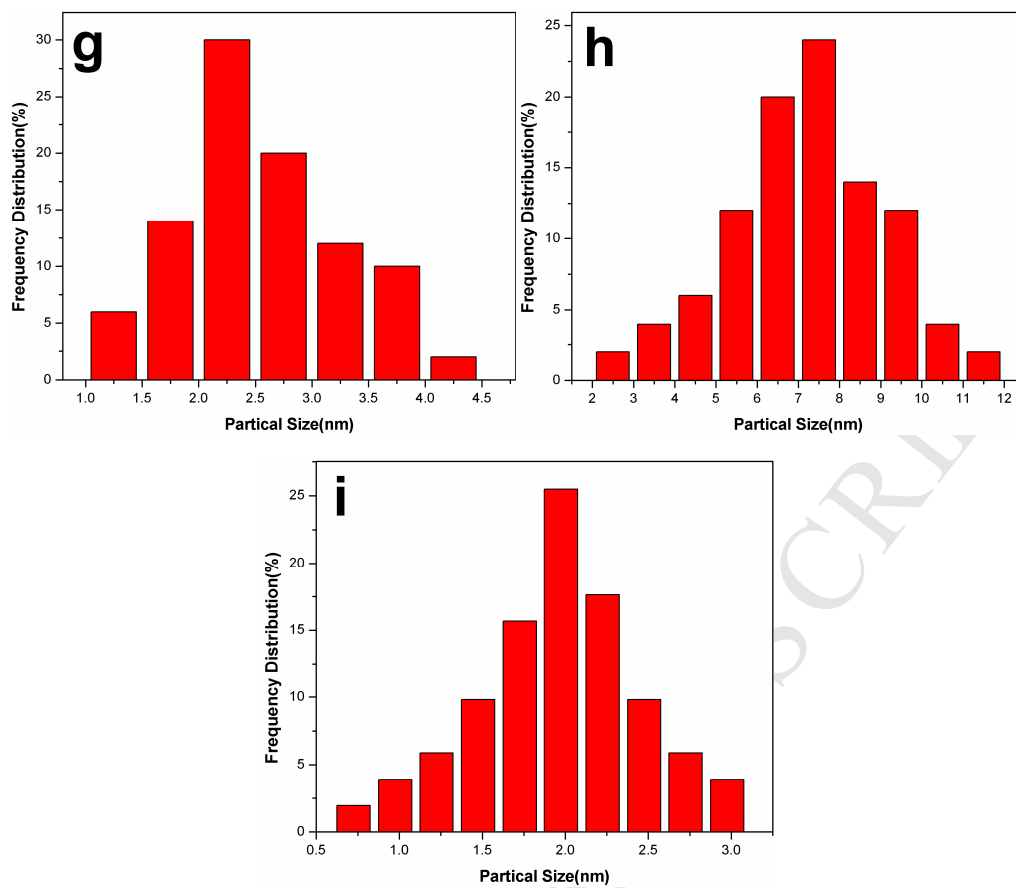
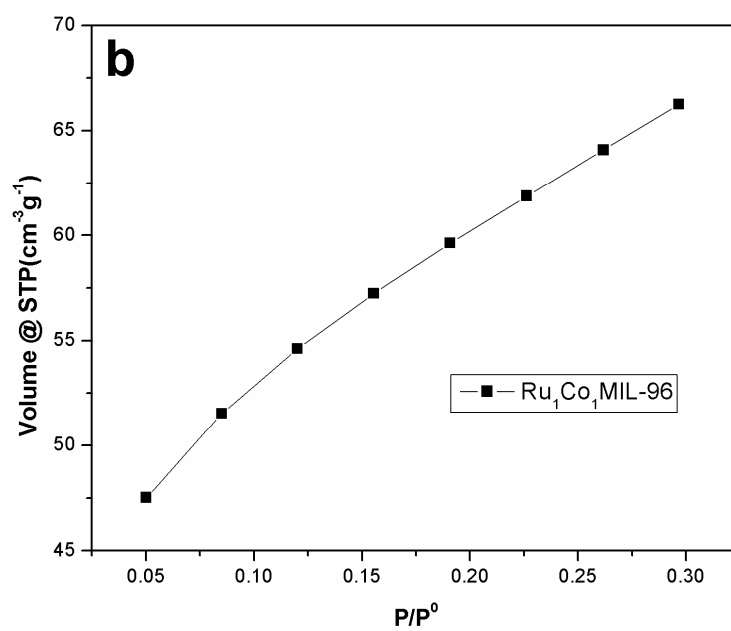
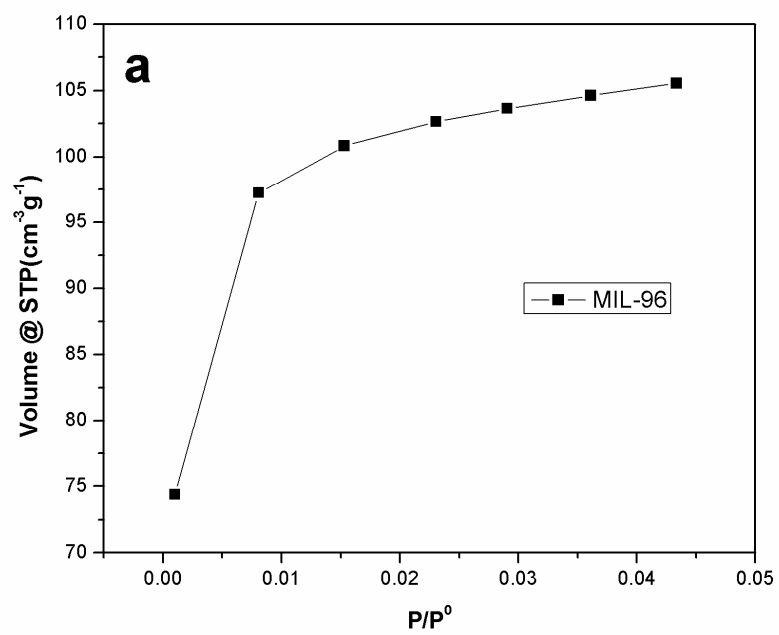


Fig. 4



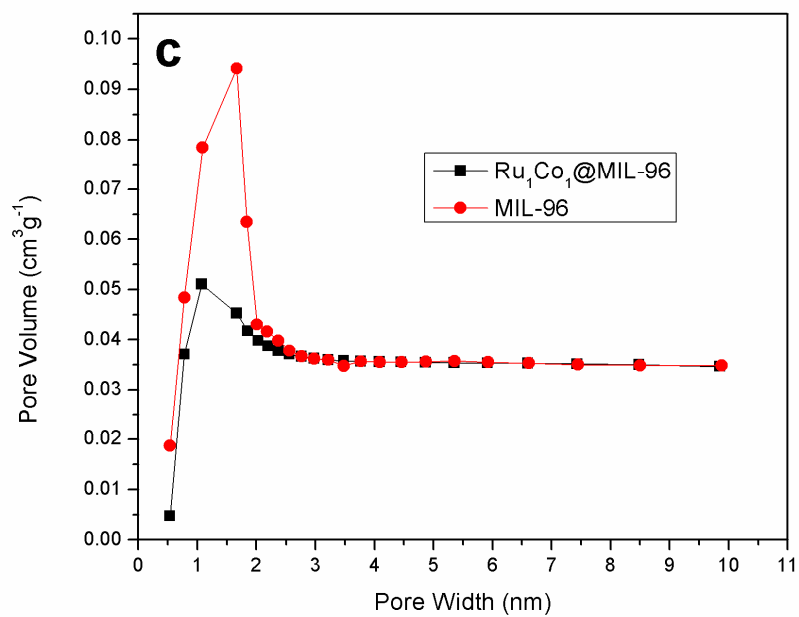


Fig. 5

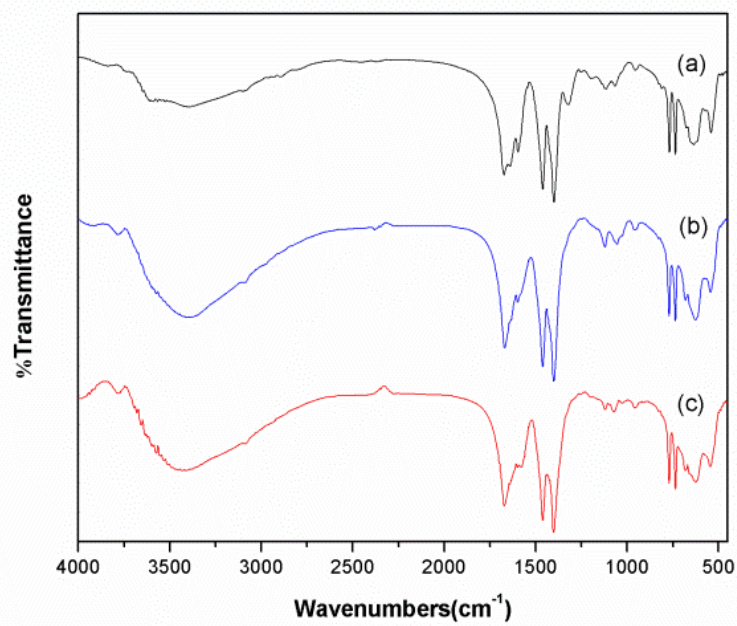


Fig. 6

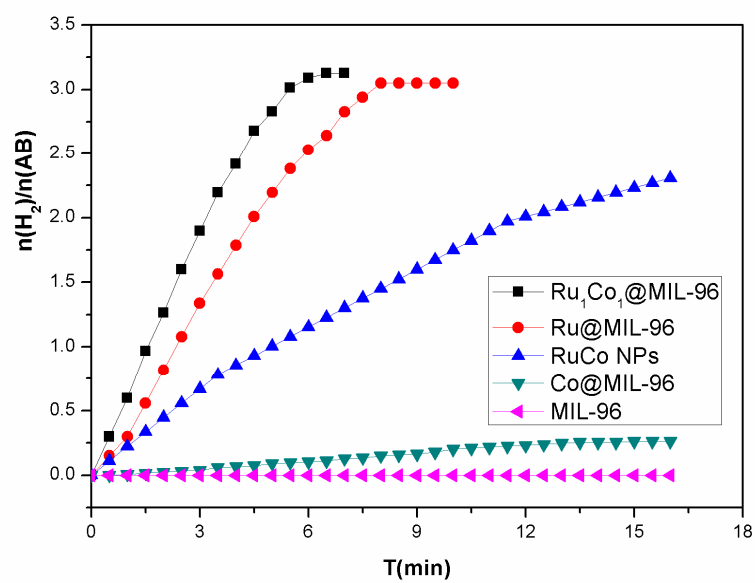
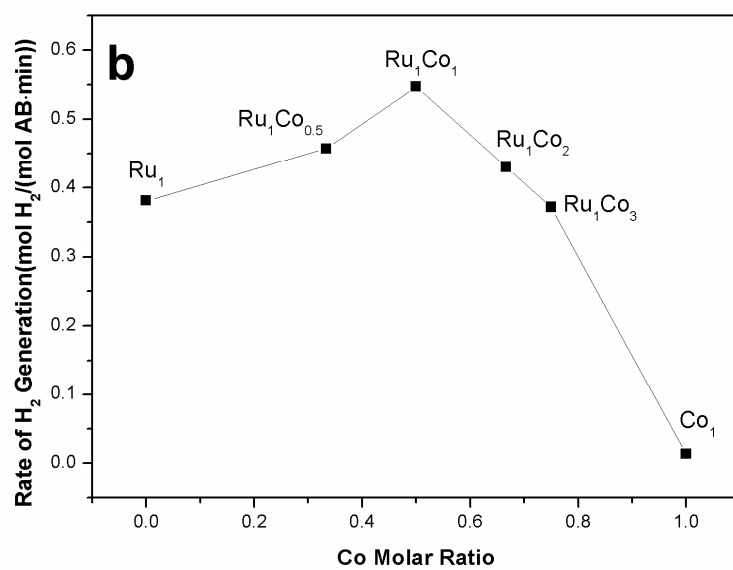
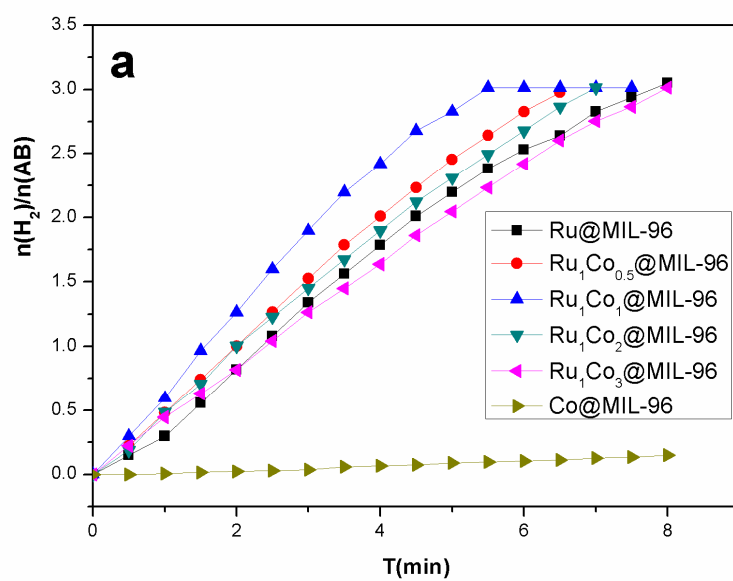


Fig. 7



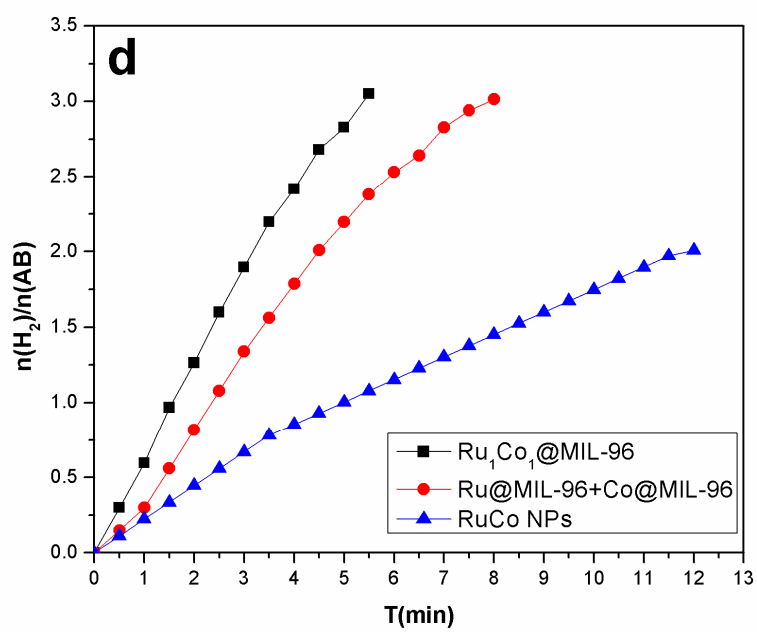
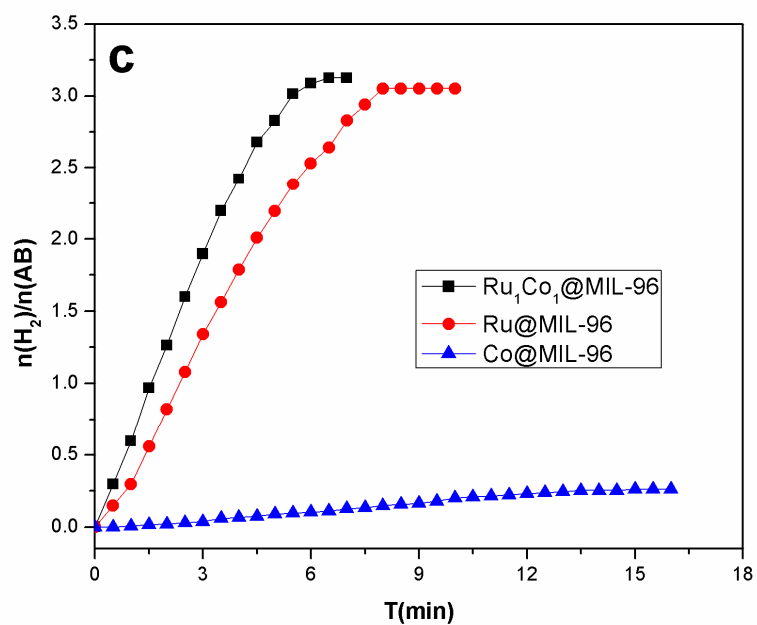


Fig. 8

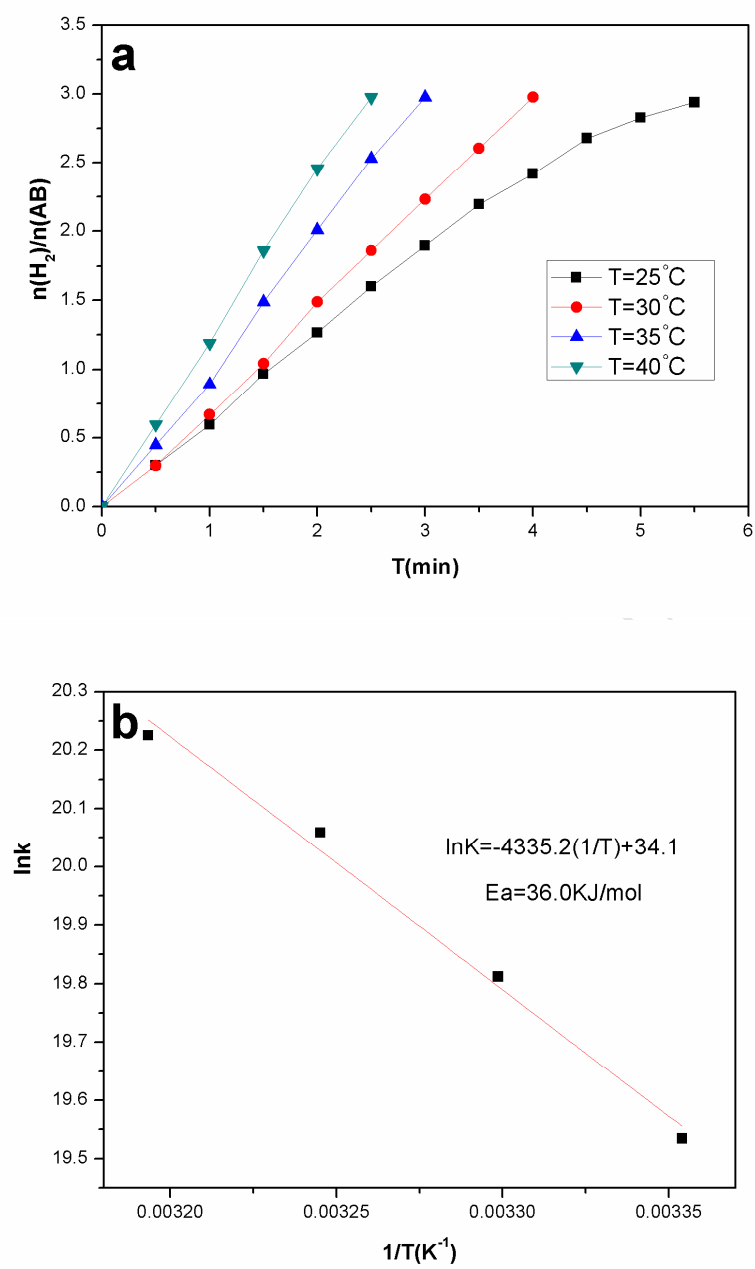
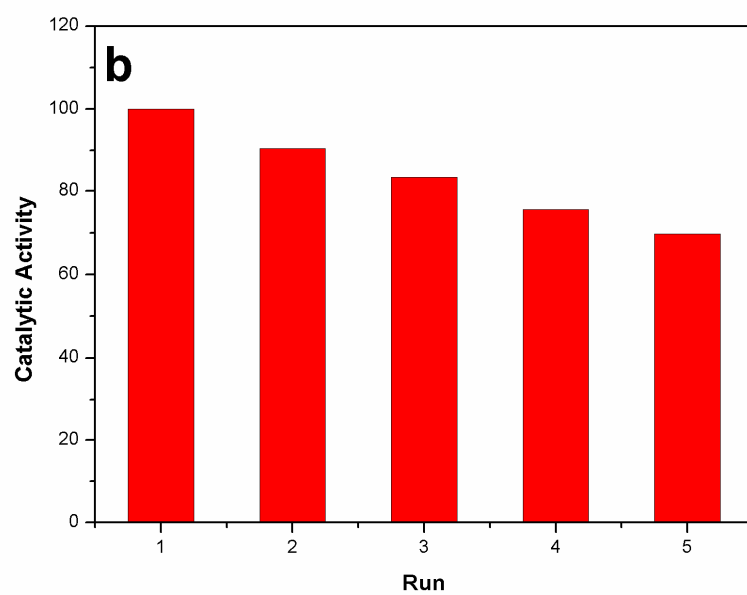
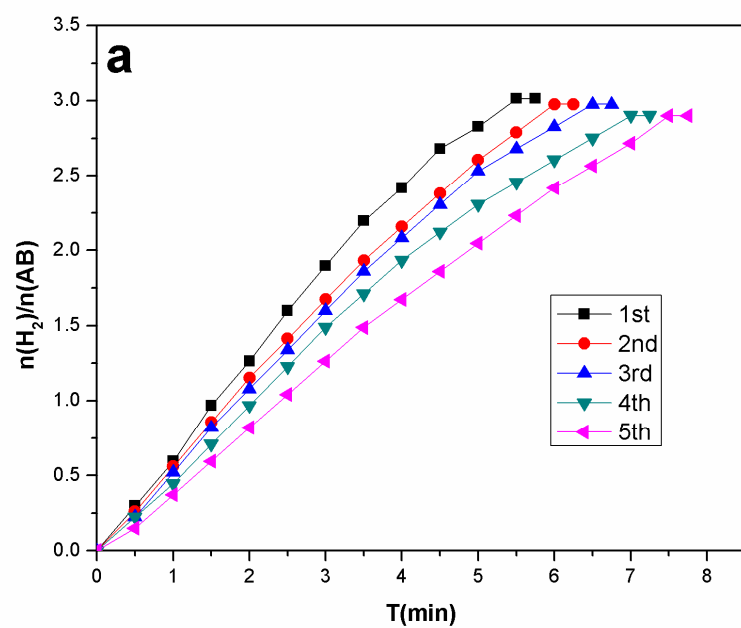


Fig. 9



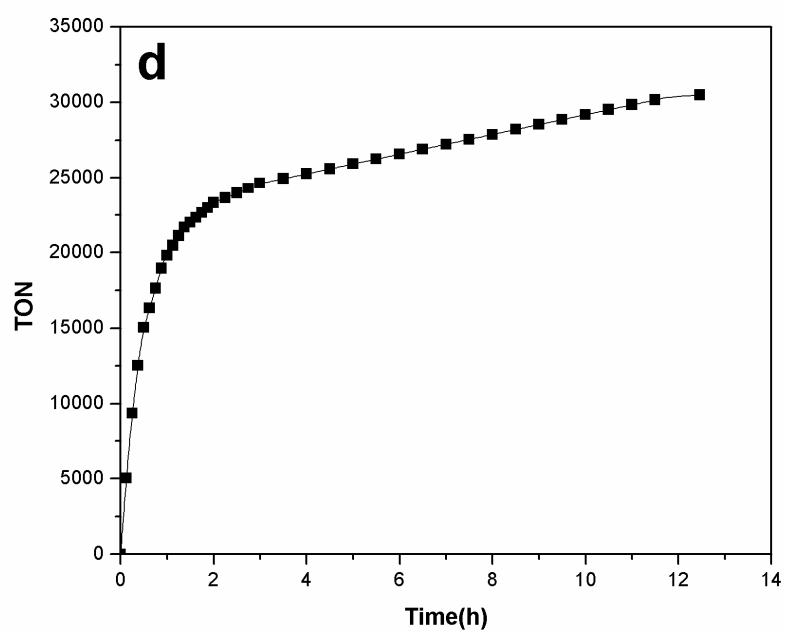
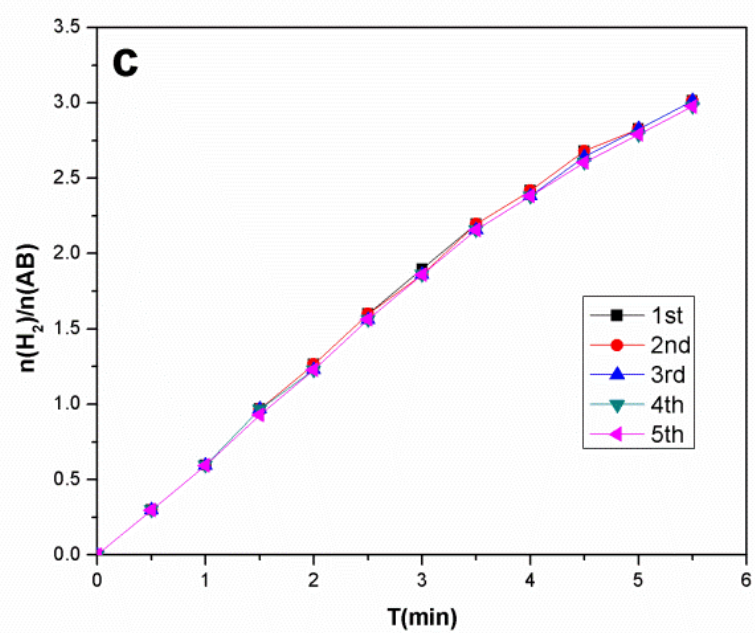


Fig. 10

Highlights

- RuCo@MIL-96 catalyst was synthesized and applied to the catalytic hydrolysis of AB.
- Ru₁Co₁@MIL-96 exhibits an excellent catalytic performance for the hydrolysis of AB.
- High catalytic activity owes to bimetallic synergistic and bi-functional effects.
- RuCo@MIL-96 catalyst is a promising candidate using as hydrogen storage material.